Thin Solid Films 778 (2023) 139908

Contents lists available at ScienceDirect

Thin Solid Films

journal homepage: www.elsevier.com/locate/tsf

Fabrication and characterization of a bifunctional zinc oxide/multiwalled carbon nanotube/ poly(3,4-ethylenedioxythiophene): Polystyrene sulfonate composite thin film

Ibolya Zita Papp [a,b], Adél Szerlauth [a,c], Tímea Szűcs [a,d], Péter Bélteky [a], Juan Fernando Gomez Perez [a,e], Zoltán Kónya [a,f], Ákos Kukovecz [a,g,*]

[a] Interdisciplinary Centre of Excellence, Department of Applied and Environmental Chemistry, University of Szeged, Rerrich Béla square 1, H-6720 Szeged, Hungary
[b] Department of Medical Chemistry, University of Szeged, Dóm square 8, H-6720 Szeged, Hungary
[c] MTA-SZTE Lendület Biocolloids Research Group, University of Szeged, 1 Rerrich B. ter, H-6720 Szeged, Hungary
[d] MTA-SZTE Lendület Computational Reaction Dynamics Research Group, University of Szeged, 1 Rerrich B. ter, H-6720 Szeged, Hungary
[e] Departamento de Ciencias Ambientales y de la Construcción, Instituto Tecnológico Metropolitano, 050034 Medellín, Colombia
[f] MTA-SZTE Reaction Kinetics and Surface Chemistry Research Group, 1 Rerrich B. ter, H-6720 Szeged, Hungary
[g] SZTE Porous Nanocomposites Research Group, University of Szeged, 1 Rerrich B. ter, H-6720 Szeged, Hungary

ARTICLE INFO

Keywords:
Nanostructure
Thin film
Semiconductor
Sensor
Ethanol

ABSTRACT

Hybrid thin film sensors based on semiconductor oxides and carbon nanostructures are promising materials to improve the sensing, thermomechanical and optical properties. In this study, a thin film based on a composite from ZnO nanoparticles, milled multiwalled carbon nanotubes, and conducting polymer was fabricated. The layer was spray-coated to the surface of amorphous polyethylene terephthalate substrate. The hybrid layer and components have been systematically characterized by transmission and scanning electron microscopy, dynamic light scattering and the optical absorption spectrum was observed by ultraviolet-visible spectroscopy. The change in glass transition temperature was measured by dynamic mechanical analysis. Gas sensing tests reveal that the ZnO/multiwalled carbon nanotube/ poly(3,4-ethylenedioxythiophene): polystyrene sulfonate film on amorphous polyethylene terephthalate has remarkably enhanced performance compared to the same layer on indium tin oxide /polyethylene terephthalate. It could detect ethanol vapor in a wide concentration range with good response, fast recovery, and repeatability at room temperature. The layer was also tested as an ultraviolet photodetector, showing a promising signal. These features indicate the composite usability in further sensor applications.

1. Introduction

In the past decade, thin conducting films have attracted extensive attention due to their application in solar panels [1], light-emitting diodes [2], photodetectors [3,4], and various gas sensors [5]. Gas and vapor sensors have numerous applications in detecting/monitoring toxic, pollutant, and harmful contaminants [6]. The concentration of VOCs (volatile organic compounds), especially ethanol, is an important parameter in human health, industrial and environmental applications such as the control of fermentation processes [7], testing of food packaging [8], exhaled breath analysis (for monitoring driving under the influence of alcohol [9,10] or as a biomarker for lung cancer [11,12]). To detect ethanol, numerous sensors have been developed [13] based on manifold sensing methods [14,15]. Portability, low cost, and low power consumption always play significant roles [16]. Conductivity measurement-based sensors containing semiconductor metal oxide nanoparticles or carbon nanotubes have the ability of forming miniature sensing systems [17]. In these thin film devices, ITO (Indium Tin Oxide) is an often used transparent conducting layer. This n-type semiconductor, prepared with SnO_2 doping of In_2O_3 has low surface resistance and a wide band gap [18]. Besides being expensive, has very poor performance under mechanical stress due to its fragile nature which opens the way for ITO substituents [19]. In the last decade, the importance of metal oxide-based sensors was shown. In this field, ZnO is a particularly often characterized n-type semiconducting oxide with a wide band gap (3.37 eV) and high exciton binding energy (~60 meV at

* Corresponding author.
E-mail address: kakos@chem.u-szeged.hu (Á. Kukovecz).

https://doi.org/10.1016/j.tsf.2023.139908
Received 18 December 2022; Received in revised form 24 May 2023; Accepted 24 May 2023
Available online 27 May 2023

room temperature), and low visible region absorption which makes it a promising material for UV (ultraviolet) photodetectors and sensor applications. In the case of ZnO photodetectors, in dark, O_2^- is forming using the electrons from the ZnO surface, resulting a depletion region. Upon exposure to UV illumination, electron-hole pairs are photogenerated, some holes desorb the adsorbed oxygen molecules from the ZnO surface to decrease the low conductivity depletion width. The unpaired photogenerated free electrons with available holes contribute to photoconduction [20]. In chemiresistive sensors, upon exposure to reductive or oxidative gasses, the resistance will change [21]. Reductive gas molecules (such as ethanol) upon interaction with the adsorbed oxygen ions on the surface of pure ZnO nanostructures can release electrons back to the conduction band, narrowing the depletion width [22] causing a measurable decrement in resistance. Although ZnO-based photodetectors and gas sensors are common in practice [23], and reportedly used in ethanol sensing in the range of 20–100 ppm but the operating temperature of these devices is usually undesirably high [24–26].

Functionalization [27] or the preparation of hybrid organic-inorganic composites [28] are effective strategies to reach higher sensor sensitivity [29,30] and lower the working temperature [31]. To improve the thermomechanical, conducting, and sensing properties of these films [32], different composites from conductive polymers, metal/semiconducting metal oxide particles [33,34], and carbon nanostructures can be used [35].

CNTs (carbon nanotubes) are often used to prepare composites [36] with polymers to reach better electrical/mechanical performances, utilizing the following properties: good conductivity, large specific surface areas, molecular-sized pores, and high adsorption capacities [37]. MWCNT (multiwalled carbon nanotube) is a preferred material in the printed electronics industry since its affordable price, ease of modification, mechanical stability, and electron mobility [38]. Due to its high aspect ratio, low dispersion ability, and high inter-tube van der Waals interaction energy, the layer preparation/printing of this material is a challenging procedure. These factors considerably restrain the stability of dispersions against aggregation-induced precipitation [39]. Different procedures can be used against aggregation such as planetary ball milling with optimized parameters to shorten MWCNTs [40] or ultrasonication, which induces defects in the nanotube's stem and even may shorten them. Battie et al. [41] and our previous studies [42] showed that the adsorption of gas particles can be affected by the number of defects in the tubes or tube ends of the carbon nanotube wall, where the defect sites can provide additional adsorption places, which could improve sensing properties. Shalaan et al. showed that when in an ethanol sensor MWCNTs were used to detect 50 ppm of the target gas, upon the exposure of reducing molecules, electrons were injected at the effective sites of CNTs' surface, then the electrons were released back when the gas was switched off. This caused first an increase and then a decrease in the measured resistance, showing the p-type behavior of CNTs [43]. Forming ZnO/CNT composite structure can increase the response dramatically and lower the optimum operating temperature for certain gasses [44]. The high aspect ratios of carbon nanotubes help to form conductive paths even at a very low concentration: CNT networks can be visualized as a network model with a tunneling effect between nanotubes [45]. Boscarino et al. prepared ZnO/CNT UV photodetectors, where the oxide is the sensitive photodetector component of the system, and CNTs play the role of the electrical transducer [46].

Conducting polymers such as poly(3,4-ethylene dioxythiophene): polystyrene sulfonate (PEDOT:PSS) [47], polyaniline, and polypyrrole have numerous advantageous properties: flexibility, conductivity, and transparency [48] which makes them combinable with semiconducting oxides and polymer substrates. PEDOT:PSS has attracted a lot of attention in recent years due to its outstanding properties such as stability, high conductivity, optical transparency in its doped state, and low band gap. PEDOT:PSS is more environmentally stable than other conducting polymers such as polypyrrole and polyaniline [49]. PET (polyethylene terephthalate) is a suitable substrate material for these thin layers due to its flexibility, transparency, and low cost [50]. The modifying effect on dielectric and thermomechanical properties of a ZnO nanorod layer on ITO-coated PET and amorphous PET (APET) substrates was previously investigated [51]. In a CNT/conducting polymer composite, percolation behavior could form conductive paths because of the interconnections between neighboring CNTs within the network [52]. Kim et al. showed, that in a PEDOT:PSS and MWCNT containing ethanol sensor, when the holes in the p-type semiconductor were depleted by the electrons from the reductive gas molecules, the decrement in conductivity was detectable [53].

During this study, utilizing the positive properties of the above-mentioned materials, the main goal was to prepare a room-temperature working and as transparent as possible sensoric thin film on a flexible polymer substrate with fast response. In this thin layer, ZnO nanoparticles were used in presence of MWCNTs and a conducting polymer (PEDOT:PSS) on a PET substrate to reach the above-mentioned properties and show an alternative to the relatively rare element containing ITO-based films as a bifunctional layer: an ethanol sensor and photodetector.

2. Materials and methods

2.1. Synthesis of nanomaterials

MWCNTs were synthesized with the CVD (chemical vapor deposition) technique [54]. To prepare CNTs, acetylene was used as a carbon source in a presence of Fe–Co/MgO catalyst. The synthesis went under an inert atmosphere for 2 h in a quartz reactor at a temperature of 650 °C.

With the CVD synthesis more than 1 μm long CNTs were prepared, which was undesirable because of the later used airbrush technique for thin film preparation: the long nanotubes could tangle and clog the equipment. Previously a wide investigation focused on the preparation of specified-sized MWCNTs by planetary ball milling [40,42]. FRITSCH P6 type ball mill was used to prepare shorter MWCNTs with more wall defects. 0.5 g of nanotubes were milled with different parameters (350/450 rpm, 20/40/60 min) in stainless steel reactor and 15, 10 mm diameter balls.

ZnO nanoparticles were prepared by the solvothermal method [55] where the Zn-precursor was zinc-acetate ($c_{(Zn\text{-}ac.)}$=0.2 M).:

$$Zn(CH_3COO)_2 + 2\ NaOH \rightarrow Zn(OH)_2 + 2\ CH_3COONa \quad (1)$$

$$Zn(OH)_2 + heat \rightarrow ZnO + H_2O \quad (2)$$

During the synthesis methanolic media was used. Sodium hydroxide solution was prepared with a concentration of 0.4 M and was added dropwise to the zinc-acetate solution during stirring. A white precipitate formed instantly ($Zn(OH)_2$) (1). The solution was thermally treated in a Teflon-lined autoclave for 6 h at 150 °C (2). Commercial amorphous PET (APET), ITO-coated PET substrates, PEDOT:PSS, reagents and solvents (purity. p.a. >99%) were pre-ordered from Sigma-Aldrich.

2.2. Fabrication of thin films

To find the best construction, different thin layers were prepared: only MWCNT, only PEDOT:PSS, MWCNT/PEDOT:PSS, and ZnO/MWCNT/PEDOT:PSS. To prepare thin films, the following solutions were prepared: 10 mg of previously milled MWCNT was sonicated in 15 ml of ethanol for 15 min. In the case of PEDOT:PSS containing samples, 10 mg of polymer pellets were dissolved in 2 ml water, then 13 ml of ethanol was added and sonicated for 15 min. When the suspension contained another solid component, 5 mg of MWCNT and 5 mg of metal oxide nanoparticles were used.

From these solutions, thin films were prepared on the surface of amorphous PET and ITO-coated PET as a reference. 20 mm x 20 mm

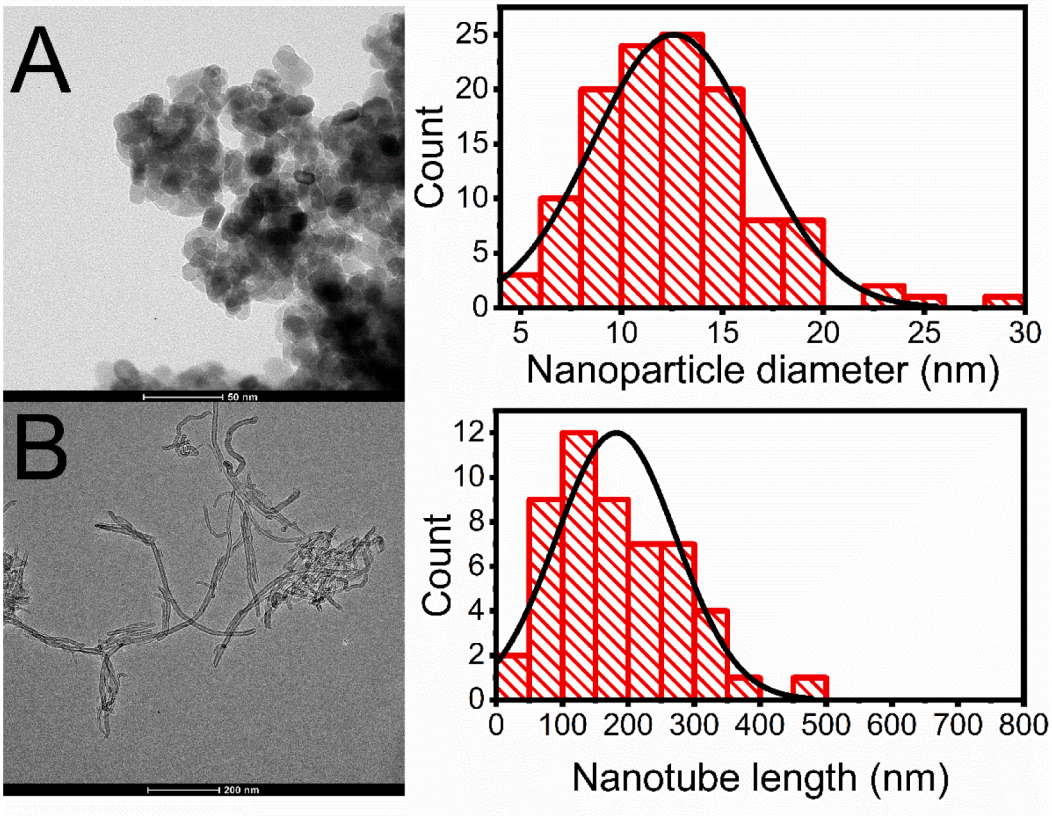

Fig. 1. TEM image and size distributions of ZnO nanoparticles (A) and milled (450 rpm, 60 min) MWCNTs (B).

squares were used from the substrates, the surface was cleaned with ethanol to remove contamination and dust. The substrate was fixed to a sample holder, which was able to move vertically with a well-defined speed. To prepare thin films, the airbrush technique was used with a fixed 100 kPa pressure N_2 gas source. To reach uniform coating, the airbrush head was attached to a motor that was able to move it horizontally. To prepare the sample, the coating method went for 10 min, and the weight of the layer was measured. This film preparation method needed brief optimization, but once good settings and parameters were reached, the prepared layers were quite uniform and homogeneous with a measured weight of 0.125 ± 0.025 mg/ 1 cm^2 surface. Dried PEDOT:PSS coatings have an average density of 1.011 g/cm^3, (for ZnO nanoparticles theoretical density is 5.606 g/cm^3 [56], 2.15 g/cm^3 for CNT [57]), which means the sample thickness is in the lower μm region or under.

2.3. Optical, structural and thermal analysis

Transmission electron microscopy (TEM) analysis was performed with an FEI Tecnai G^2 20 X-TWIN instrument (operating voltage: 200 kV) with a point resolution of 0.26 nm on the synthesized nanoparticles. Samples were placed on carbon-coated copper grids of 300 mesh. Quantitative image analysis was performed by ImageJ. Before thin film preparation, sedimentation was observed to find a compatible solvent and MWCNT length. Zetasizer Nano ZS type instrument was used with quartz cuvettes to measure the polydispersity indexes and Zeta potentials of carbon nanotube samples. Morphological and structural analysis of the coatings was performed using a Hitachi S4700 scanning electron microscope (SEM) operated at 10 kV accelerating voltage and 10 μA emission current and a Thermoscientific Apreo C SEM (10 kV accelerating voltage and 1 pA emission current). For transmittance analysis of coated and neat films, an Ocean Optics UV–Vis spectrometer with a USB-4000 type detector with a light source of DH-2000-BAL (deuterium-halogen lamps) was used. Dynamic mechanical measurements were performed on TA Instruments Q800 equipment. Glass transition temperatures (T_g) were determined from tan δ curves using a Tension:Film clamp in a region of 25–150 °C with a heating rate of 3 °C/min applying a constant 1 Hz frequency (amplitude: 10 μm, preload: 0,01 N).

2.4. Sensor measurements

Before testing the film as a sensor, drops of conductive silver paste were placed to the samples, 10 mm apart to provide the electric conductivity between the electrodes and the surface. The sensing performance was evaluated under laboratory conditions (25 °C, atmospheric pressure). To perform sensory measurements, LabJack UE9 for control with a Keithley A Tetronix Company 2401 Source Meter, GFC17 – AALBORG Mass Flow Controllers, an AALBORG Command Module and a cylindrical Linkam HFS600E test chamber (calculated volume= 150 mL) were used. Further description of the sensor setup is provided later (Fig. 5). For photodetecting measurement, as a UV light source, a commercial UV LED (Light Emitting Diode) was used (Operating properties: 3 – 3.4 V, 20 mA, 300–400 mCd, 395–400 nm).

3. Results and discussion

3.1. Nanoparticle and thin layer characterization

Fig. 1. illustrates the TEM pictures and quantitative particle size distribution analysis of the prepared nanostructures. During the solvothermal synthesis of zinc-oxide NPs, sphere-shaped nanoparticles were formed with an average diameter of 12 nm (median: 12 nm). Transmission electron microscopy images show the differences between carbon nanotube samples milled with different parameters. The carbon nanotubes without milling had micrometer lengths. The milled nanotubes, when the cumulative milling energy was the smallest (350 rpm,

Table 1
Results of DLS (Dynamic Light Scattering) measurements and average nanotube lengths from TEM.

Milling time of MWCNTs	Average nanotube length (nm) (TEM)	Polydispersity index	Zeta potential (mV)
350 rpm 20 min	449	0.418	−23.9
350 rpm 40 min	274	0.878	2.47
350 rpm 60 min	268	0.795	−24.8
450 rpm 60 min	181	0.686	−33.1

20 min) had an average length of around 450 nm. By varying the milling parameters, a change in the length of the nanotubes can be observed: with higher milling energy (450 rpm, 60 min) the resulting average nanotube length was 181 nm. The results are summarized in Table 1.

For further applications, not just the proper CNT length was important, it was needed to find a solvent that is compatible with the surface of the substrate, and can be used to prepare thin layers, besides avoiding aggregation which causes sedimentation/clogging during the film preparation. To ensure these properties, different types of solvents were tested. Based on the observations of sedimentation, ethanol was chosen for further preparations. This alcohol is compatible with the substrate and showed the best stability with milled nanotubes. The importance of nanotube length was also noticeable: while the non-milled sample settled rapidly, the 450 rpm/60 min milled nanotubes showed slower sedimentation.

Zeta potential is a term for electrokinetic potential in the case of colloidal dispersions: the magnitude of this potential indicates the degree of electrostatic repulsion between adjacent, similarly charged particles in a dispersion. If the particle size is small enough, a high zeta potential will predict stability, which indicates that the solution will resist aggregation [58]. In the case of ethanol, the best results were shown for the 450 rpm/60 min milled nanotubes, where the absolute value of the Zeta potential is the highest which suggests higher stability in the media, so for the preparation of films, 450 rpm/60 min milled MWCNTs and ethanol as a solvent were chosen.

Scanning electron microscope images show a difference between the coated samples. The only zinc oxide-containing film has a homogeneous distribution of particles, samples with PEDOT: PSS and MWCNT showed larger aggregates on the SEM scans.

The close-up SEM images showed that a part of the applied particles was aggregated, in the conducting polymer layer, metal oxide, and carbon nanoparticles can be observed. The surface of the aggregated particles is usually covered with nanotubes and ZnO (Fig. 2/A and /B). Characterization of ZnO/MWCNT/PEDOT:PSS film, prepared on APET by energy dispersive X-ray spectroscopy (EDS) showed the presence of C, O, Zn, S, and Au (Fig. 2/D) where artificial green coloring was used to show Zn (Fig. 2/C). Au signal originated from the previously prepared gold layer.

Fig. 3/A shows a complete cross-sectional view of the substrate and the prepared thin film embedded in epoxy, to stabilize the sample for cutting. On the surface of the APET substrate (thickness: 248 μm), when a line scan for Zn was performed, the measured thin film thickness was 1.25 μm. It is important to notice, that it only shows the distance, where Zn signal is detectable, which is originated to ZnO nanoparticles, but bigger aggregates could cause a difference in layer thickness. The prepared composite thin film and components are observable on Fig. 3/B, C and D.

UV–Vis transmittance measurements showed that pristine APET substrate has a transmittance of around 80%, for ITO coated PET substrate (ITO/PET) this value is a bit lower. For each coated sample, it can

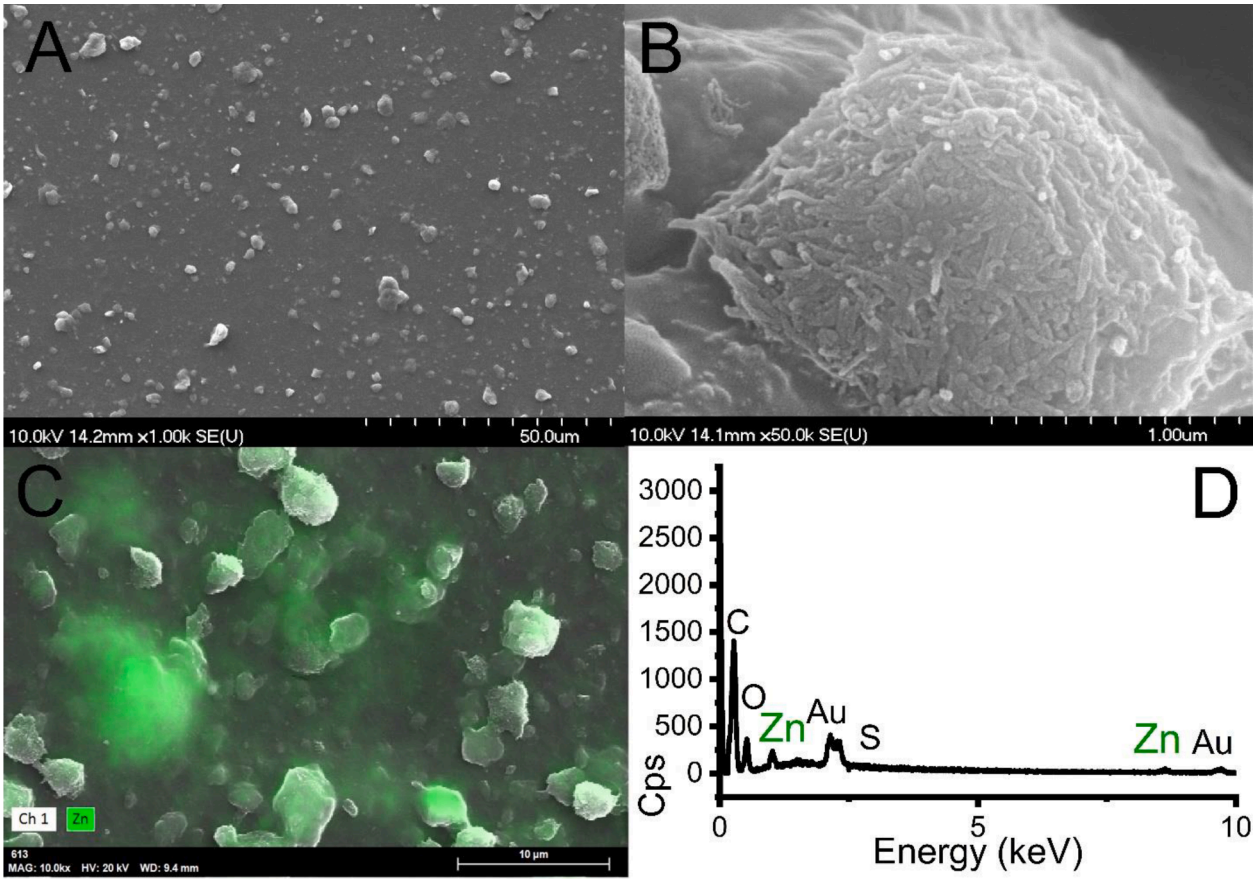

Fig. 2. SEM images of the ZnO/MWCNT/PEDOT:PSS layer surface with 10 kV (A, B), color mapping of the surface where green color corresponds to Zn, with 20 kV (C) and the EDS spectrum of the ZnO/PEDOT:PSS/MWCNT layer on APET (D).

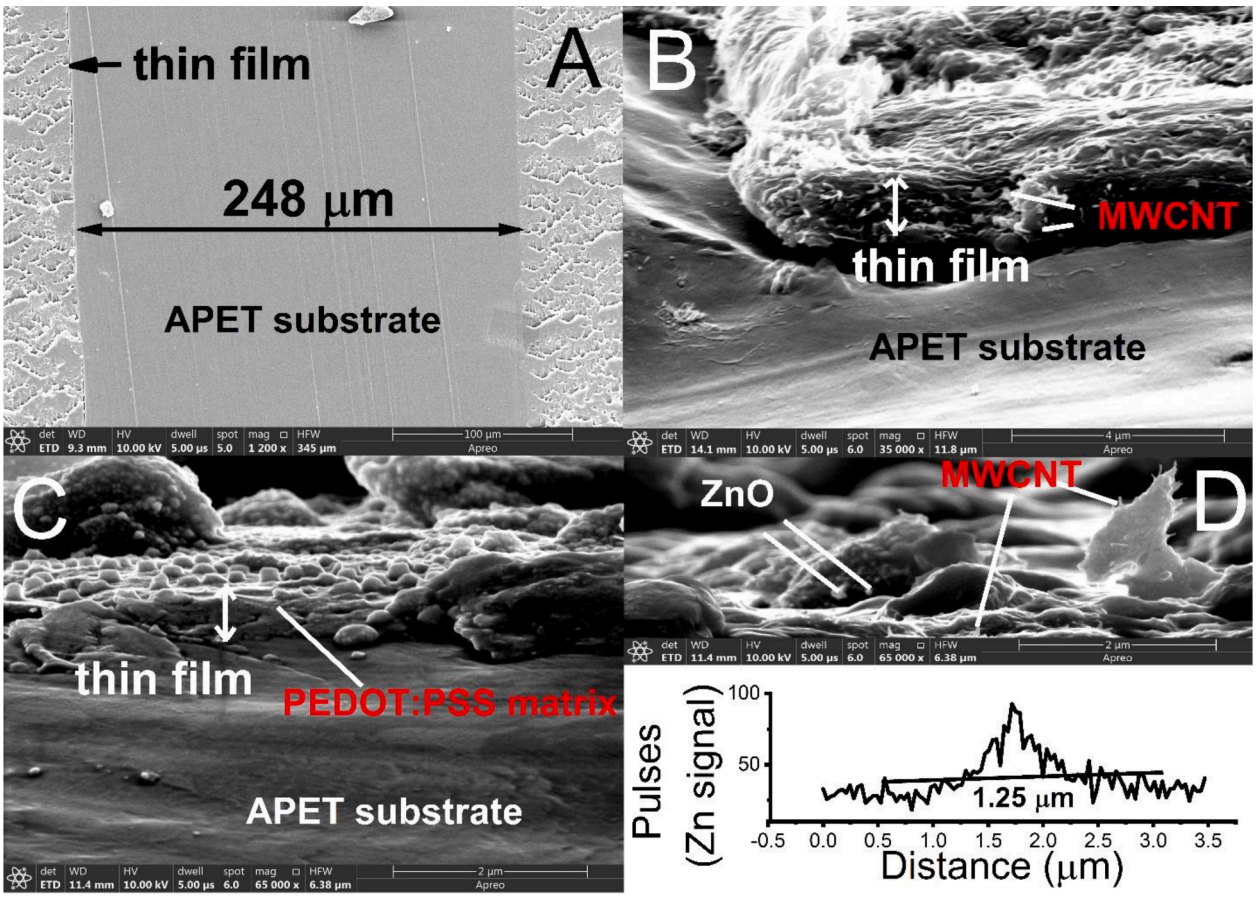

Fig. 3. Cross-sectional SEM image from the whole APET substrate and layer, embedded in epoxy (A), the ZnO/MWCNT/PEDOT:PSS thin film on APET surface (B), cross section SEM image from the thin film and the substrate (C, D) and line scan results for ZnO.

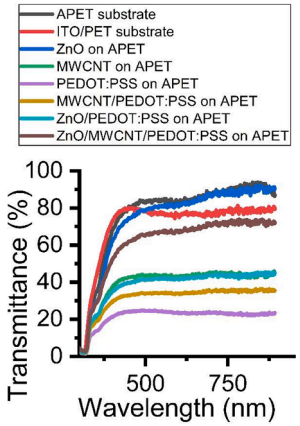

Fig. 4. Transmittance spectra of APET-based thin films compared to neat APET and ITO/PET substrates.

be stated that the coatings reduced transparency. The measured transmittance only in two cases exceeded the substrate's value. Among these thin films, besides the thin ZnO film, which closely approximated the transmittance of neat APET, the APET-based ZnO /MWCNT/PEDOT:PSS composite still had outstanding properties, as its transmittance exceeded 60% (Fig. 4).

Oscillatory DMA (Dynamic Mechanical Analysis) measurements provide information about the viscoelastic properties of a material. The glass transition temperatures were determined from the tan δ peak maximum at a specific frequency. The measured values are presented in

Table 2
The measured T_g values (DMA precision: ±1%).

Sprayed-on layer	T_g (°C) ITO/PET substrate	T_g (°C) APET subsrate
neat substrate	127.9	91.9
ZnO	125.5	96.4
MWCNT	127.6	100.2
PEDOT:PSS	126.1	102.5
MWCNT/PEDOT:PSS	125.6	101.4
ZnO/PEDOT:PSS	130.4	99.9
ZnO/MWCNT/PEDOT:PSS	125.4	100.0

Table 2. When the APET substrate was used, all the thin films caused an increment in the glass transition temperature. However, in the case of ITO/PET-based samples, there is not such a positive difference between the substrate and the film-containing samples: only the ZnO/PEDOT:PSS layer caused higher T_g values. About the APET-based samples, it is visible that we were able to increase the T_g in all cases, so we improved this thermal-mechanical property compared to the neat substrate. In addition, it is observable that the APET substrate has a lower T_g value than ITO/PET, caused by its level of amorphicity.

3.2. Sensing properties

Before placing the samples into the test chamber, conductivity was always tested by placing the multimeter electrodes on the silver drops. The chamber temperature was set to 25 °C, the constant flow rate was 200 mL/min. The first step was to obtain the I-V characteristics between −5 and + 5 V, with 25 measuring points. The ITO/PET substrate obviously showed a linear I-V curve. The linear I–V characteristics indicate

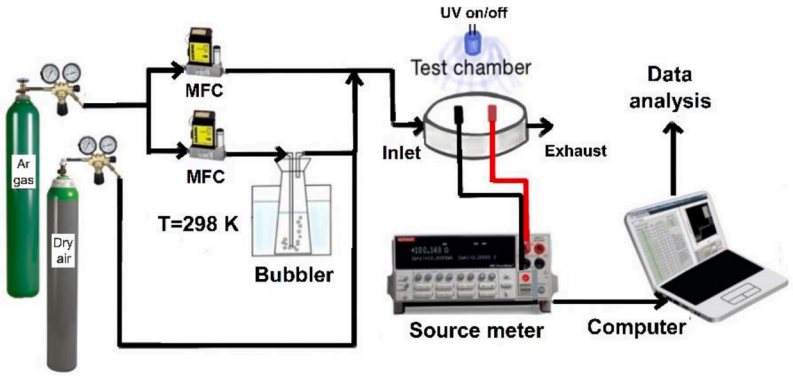

Fig. 5. Instrumental setup for sensor measurements.

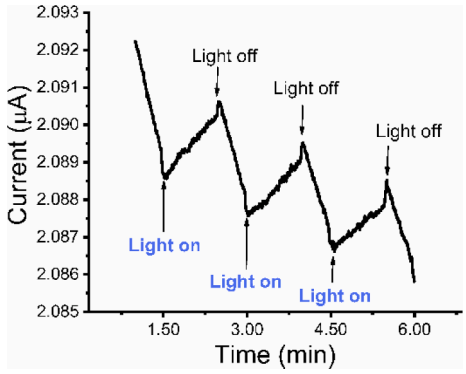

Fig. 6. Measured UV photoresponse characteristics of ZnO/MWCNT/PEDOT:PSS layer on APET substrate.

good ohmic contacts with no interfacial barrier or traps between the sensing film. None of the samples prepared on the ITO/PET surface exceeded its good conductivity, however, PEDOT:PSS/MWCNT, and ZnO/MWCNT/PEDOT:PSS layers approached it. APET is basically a non-conducting material, but when PEDOT:PSS, MWCNT/PEDOT:PSS, and ZnO/MWCNT/PEDOT:PSS films were present, promising I-V characteristics were shown. Fig. 7/A. shows the I-V curves for ZnO/MWCNT/PEDOT:PSS layer compared to the neat substrate, APET. The ohmic behavior of contacts ensures that each surface resistance change is due to the tested target.

Mass flow controllers (MFCs) were used to set the flow rate of dry air, Argon, the carrier gas, and ethanol vapor, the target, respectively. A PC was connected to the testing circuit to monitor and record the electrical resistance (Fig. 5). The vapor concentration in the test chamber was controlled by the MFCs and valves where controllers were set to the 200 mL/min flow rate. The accuracy of the flow adjusting reported by the manufacturer is ±1%, so the precision of the concentration is ±1 ppm in the case of the maximum added ethanol vapor, respectively. A switchable commercial UV LED on the top of the test chamber was used as a UV source.

As Fig. 6. shows, by repeatedly turning the UV source on and off, a detectable signal was reached, proving the photosensitive properties of the ZnO/MWCNT/PEDOT:PSS layer. In absence of UV light, the surrounding oxygen molecules adsorb to the ZnO surface, removing the free electrons, creating a depletion region, resulting a reduced conduction. In the presence of UV light, electron-hole pairs are forming by the absorption of photons and flowing through the depletion region, an increment in current is observable. Holes are attracted to oxygen ions to neutralize them, after that, when an oxygen molecule is released, free electrons cause the increment in conductivity (Fig. 8/A.). Choi et al. showed how the addition of MWCNTs could improve photodetecting. With the formation of p-n heterojunction (hole depletion and enriched electrons between ZnO and CNTs), the stability of free electrons and the electric transport through a highly conductive CNT matrix [59] could improve, which effectively guides the photocarrier movement which in our case was supported by the PEDOT:PSS, as a hole transporter.

During the ethanol sensor measurements, ZnO/MWCNT/PEDOT:PSS coating on APET substrate was tested under the following circumstances: 90 s exposure time was followed by 15 min recovery time. The same concentration (49.4 ppm ±1%) of ethanol vapor reached the surface three times in a row, to follow recoverability. It is visible that the ITO layer is not needed at all: the prepared composite layer is suitable for detection, the prepared thin layer with high transparency showed good results (Fig. 7/B.). The sensor response can be defined as R_a/R_g for reducing gasses or R_g/R_a for oxidizing gasses, where R_a is the resistance of gas sensors in the reference gas (usually the air or inert gas) and R_g stands for the resistance in the target gasses [60]. The response time and recovery time were defined as the time to reach 70% of the total resistance change [61].

The following set of measurements was made by changing the ethanol vapor concentration per cycle, so 100% (98.8 ppm ±1%) EtOH flow was added to the sample for the first 90 s, then 75% (74.1 ppm ±1%) after a 15-minute break, again for 90 s, 50% (49.4 ppm ±1%) again after 15 min. only 25% (24.7 ppm ±1%) in the last cycle (Fig. 7/C.).

Fig. 7/D. shows the concentration dependence of the signal: from integrated peak areas, using a calibration set, the unknown ethanol concentration on the sample is predictable (R^2=0.9898). The prepared thin ZnO/MWCNT/PEDOT:PSS layer showed linear sensitivity in the measured region. The increment of sample thickness is not necessary: it causes non-linear characteristics and a signal shift. Response time was 7.2 s for the thin ZnO/MWCNT/PEDOT:PSS on APET with a recovery time of 32.1 s with a sensitivity of 122 μΩ/ppm (and S%=2.3% to 98.8 ppm ethanol). (The same layer on ITO/PET substrate -which was measured for comparison- had a response time of 24.8 s and recovery time of 121 s, with high noise level and low sensitivity). Sensitivity was defined as the ratio between the changes in sensor response over a change in vapor concentration (3):

$$S = \left[\left(\frac{Ra}{Rg_2}\right) - \frac{Ra}{Rg_1}\right]/(c_2 - c_1) \quad (3)$$

The prepared highly transparent ZnO/MWCNT/PEDOT:PSS hybrid layer on a flexible APET substrate showed a lower response time than pure ZnO-based sensors (Table 3.) but its sensitivity in the measured composition was lower, however, the device worked without any heating. The measured concentration range is comparable with the literature. Recovery times are lower than in MWCNT/PEDOT:PSS samples and the results are closer to the previously reported CNT/ZnO composites. Room temperature usability is advantageous in low-power consumption applications.

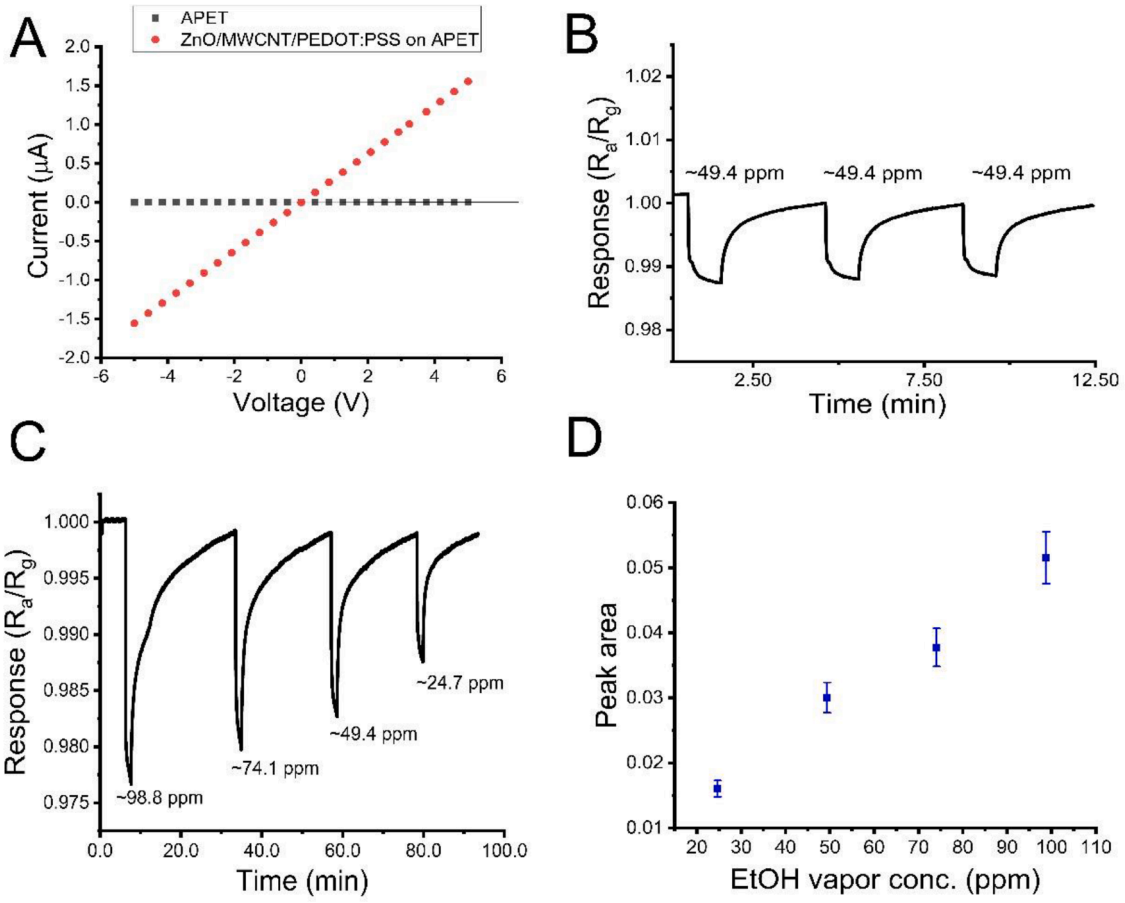

Fig. 7. (A) I-V curves of ZnO/MWCNT/PEDOT:PSS layers. (B) Dynamic response curves of the ZnO/MWCNT/PEDOT:PSS layer on APET for ethanol. (C-D) Dynamic response curves and integrated peak areas of the ZnO/MWCNT/PEDOT:PSS on APET substrate, exposure to different ethanol concentrations at room temperature.

Table 3
Sensing properties compared with different ethanol sensors from the literature.

Sample	Working temp. (°C)	Operating voltage (V)	Measured concentration or range (ppm)	Response time ($t_{70\%}$ or $t_{90\%}$, s)	Recovery time (s)
ZnO NPs [62]	200	–	200	35	29
ZnO/SnO_2 [63]	300	–	0.5–100	72	120
MWCNT/PEDOT:PSS [53]	RT.	5	400	18	59
CNT-ZnO/PS [64]	RT.	–	500	18	29
MWCNT [43]	30–60		50	40	–
ZnO_2/PAA/ZnO_2/SF [65]	RT.	–	0.48–11.9	40	80
ZnO_2 hybrid [66]	RT.	–	10–100	50	110
ZnO/MWCNT/PEDOT:PSS on ITO/PET	RT	5	49.4	25	121
ZnO/MWCNT/PEDOT:PSS on APET (This work)	RT.	5	24.7–98.8	7	32

3.3. Ethanol sensing mechanism

According to Yamazoe [67], a gas sensor consists of two basic functions: receptor and transducer. The receptor function includes the recognition of the target substance, transducer function is needed to convert the chemical change into a detectable electrical signal. Sensor response and recovery are based on the mechanism when target gas molecules adsorb onto or desorb from the sensor material surface, which causes its change in resistivity. Semiconductor nanomaterials have the required high surface-to-volume ratio and high mobility of electrons which is beneficial for the sensing mechanism [68]. It is known, when only n-type ZnO is used as sensor material, at higher working temperatures, and reducing molecules reach the surface, the previously formed oxygen species would react with the reducing target [69], decreasing the potential barrier and allowing electrons flow more easily, causing the decrement of the measured resistance.

In contrast, MWCNTs behave as a p-type semiconductor, upon exposure to a reductive target, the transferred electrons will recombine with hole carriers, reducing the concentration of charge carriers, increasing the depletion layer and the potential barrier height causing an increment in electrical resistance [70]. PEDOT:PSS is a heavily doped, also p-type semiconductor, where holes on the $PEDOT^+$ chains are compensated by sulfonate anions on the PSS^- chains (dopant) [71] and have been proposed for their use as hole transporters. ZnO is proven to be able to form p-n heterojunctions with MWCNT which can improve the electrical properties [72]. Numerous p-n type junctions have been formed previously: Talib et al. fabricated ZnO nanorod/polyaniline p-n junctions on flexible substrates which showed a high sensitivity of 85% whereas the photodetectors showed quantum efficiency as high as 12% [73]. Ghushe et al. suggest that in MWCNT-doped ZnO/organic p-n

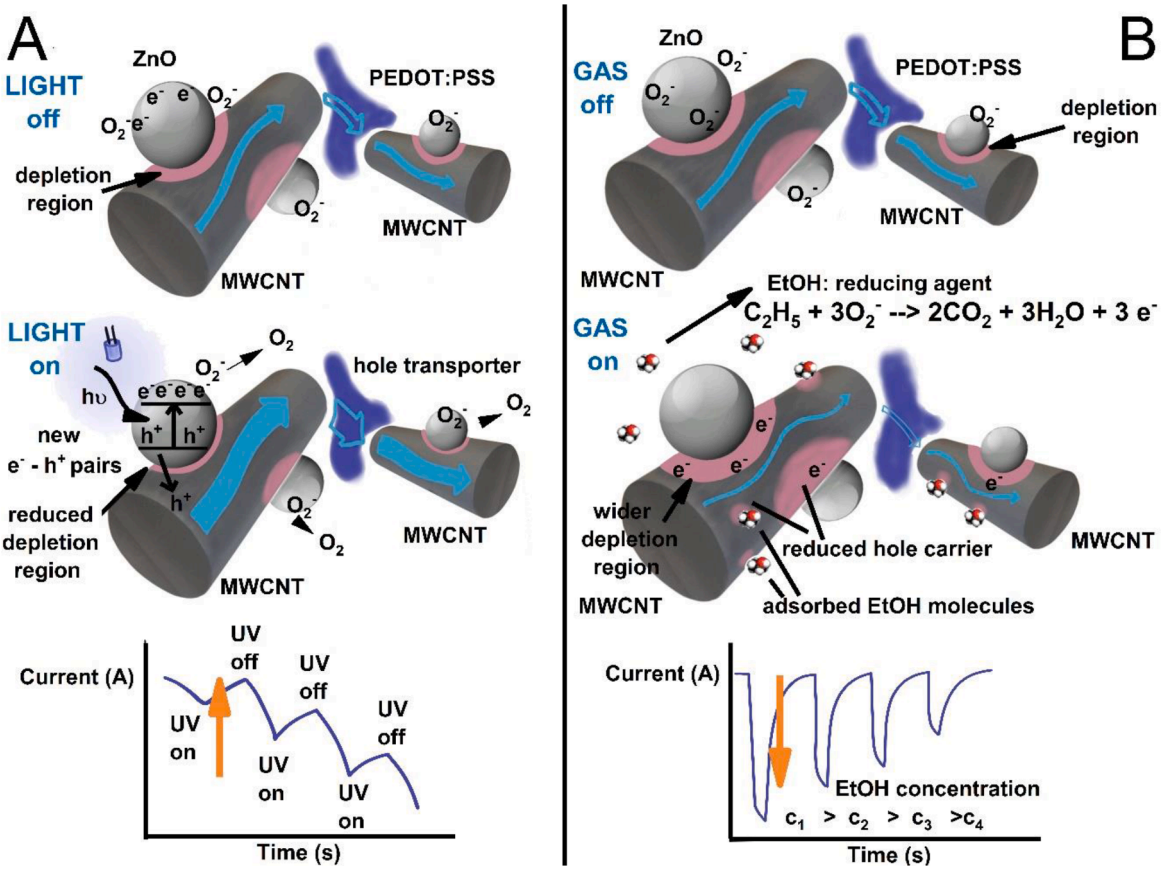

Fig. 8. Schematic illustration of UV photodetecting (A) and ethanol sensing (B) mechanism.

heterojunctions, MWCNTs facilitate the charge transfer at the interface resulting in lowering barrier heights as compared to other heterojunctions [74]. At the interface, holes from p-type polymer and MWCNT nanocomposite and electrons from n-type ZnO nanoparticles could take place during junction formation. Sinha et al. reported a ZnO/MWCNT-based n-p switchable sensor, where they proved that in a lower temperature range the layer showed p-type characteristics [75]. Similar results were reported in the case of ZnO-doped MWCNT gas sensors [76] and other n-p heterojunctions [77,78]. In these junctions, upon exposure to reductive gas, the target molecule reacts with the previously formed O_2^- ions on the ZnO surface, providing free electrons, widening the depletion region resulting in a decrement of conductivity.

Since the addition of reducing gas to our test chamber reduced the conductivity, two possible reaction routes could take place. Besides at room temperature the CNT surface behaves like a p-type semiconductor (its resistance increases upon exposure to reducing gas due to lone pair electron transfer from ethanol to the valence band causing the decrement of hole carrier concentration [53]) it is also possible that a p-n heterojunction formed between ZnO nanoparticles and MWCNTs where PEDOT:PSS helped the conductivity as a flexible conducting matrix and a hole transporter (Fig. 8/B.). Overall at room temperature, the thin film exhibits p-type semiconducting behavior and is dominated by positive charge carriers (holes), whereas the adsorbed reducing molecules on the film surface serve as electron donors [79], causing the reduction of holes, increasing the film resistance. That means the observed sensoric properties for reducing organic vapor are mostly based on the p-type CNT gas sensor characteristics, which is a typical behavior for CNT/ZnO-based sensors at room temperature [80,81]. Septiani et al. also showed that in the lower temperature region, ZnO/MWCNT heterojunctions showed p-type behavior while sensing reductive target, suggesting that the primary sensing mechanism in this region is mainly based on the physisorption of the target gas on the MWCNT surface [82]. In this mechanism, the specific surface area is an important factor, so during the sample preparation, the milling of MWCNTs not just made easier the spray coating of films, but provided more adsorption position for target molecules.

In our composite layer, the other phenomenon which could reduce the response time is the previously mentioned percolation effect between the PEDOT:PSS and MWCNT-ZnO heterojunctions. This could help form conductive paths between neighboring CNTs within the network [52]. Since in p-type semiconductors the behavior is dominated by the positive charge carriers, the addition of the conducting polymer, a typical hole transporter could provide a faster sensor response.

4. Conclusions

In summary, hybrid thin layers of ZnO nanoparticles, milled carbon nanotubes, and conductive polymer (PEDOT: PSS) were prepared on amorphous polyethylene terephthalate (APET) and ITO-coated PET substrates. As a first step, carbon nanotubes and ZnO nanoparticles were synthesized. Before the film preparation, the optimal solvents and milling parameters of nanotubes were determined by using TEM and DLS measurements to avoid aggregation and provide defects on nanotubes to increase the number of adsorption places. SEM/EDS images showed the surface characteristics and layer integrity of airbrush-prepared thin films. UV–Vis measurements showed that the ZnO/MWCNT/PEDOT:PSS layer on the APET substrate exceeded more than 60% transmittance in the visible region. The change in glass transition temperatures (T_g) was investigated by dynamic mechanical analysis. Results showed, that all the prepared thin layers on APET substrates caused an increment in T_g values, which indicates a higher resistance of the material against thermomechanical effects. ZnO/MWCNT/PEDOT:PSS thin film on APET substrate showed good response to UV light as a photodetector and also to ethanol vapor: the films were recoverable and

the signal was concentration-dependent. During UV irradiation, the conductivity increased, indicating an n-p heterojunction formation whilst the interaction with reductive target gas caused an increment in resistance, proving a p-type sensing mechanism where the conducting polymer as a hole transporter helped to reduce the response time. Although more parameters await refinement, these results suggest the room temperature sensor applicability of this bifunctional composite material.

CRediT authorship contribution statement

Ibolya Zita Papp: Conceptualization, Writing – original draft, Methodology, Investigation. **Adél Szerlauth:** Investigation. **Tímea Szűcs:** Investigation. **Péter Bélteky:** Investigation. **Juan Fernando Gomez Perez:** Investigation. **Zoltán Kónya:** Supervision, Funding acquisition. **Ákos Kukovecz:** Conceptualization, Writing – review & editing, Resources, Funding acquisition.

Declaration of Competing Interest

The authors declare that they have no known competing financial interests or personal relationships that could have appeared to influence the work reported in this paper.

Data availability

Data will be made available on request.

Acknowledgments

Project no. RRF-2.3.1-21-2022-00009, titled National Laboratory for Renewable Energy has been implemented with the support provided by the Recovery and Resilience Facility of the European Union within the framework of Programme Széchenyi Plan Plus.

References

[1] M.W. Alam, M. Ansari, M. Aamir, M. Waheed-Ur-Rehman, N. Parveen, S. Ansari, Preparation and characterization of Cu and Al Doped ZnO thin films for solar cell applications, Cryst. 12 (2022) 128, https://doi.org/10.3390/cryst12020128.
[2] H. Zhang, J. Mischke, W. Mertin, G. Bacher, Graphene as a transparent conductive electrode in GaN-Based LEDs, Materials 15 (2022) 2203, https://doi.org/10.3390/ma15062203.
[3] A. Kyriakis, N. Glezos, D. Velessiotis, G. Pilatos, T. Speliotis, A. Stefanou, A UV photodetector based on ordered free standing MWCNT, J. Instrum. 15 (2020) C01015, https://doi.org/10.1088/1748-0221/15/01/C01015.
[4] R.A. Ismail, A.D. Faisal, S.S. Shaker, Preparation of ZnS-decorated MWCNTs/p-Si hybrid photodetector by pulsed laser deposition, Opt. Mater. 133 (2022), 112998, https://doi.org/10.1016/j.optmat.2022.112998.
[5] V. Elanjeitsenni, K.S. Vadivu, B. Prasanth, A review on thin films, conducting polymers as sensor devices, Mater. Res. Express 9 (2022), https://doi.org/10.1088/2053-1591/ac4aa1.
[6] A. Gaiardo, E. Demenev, P. Tosato, P. Bellutti, C. Dolci, A. Maestrini, F. Antonelli, V. Miotto, New chemoresistive gas sensor arrays for outdoor air quality monitoring: a combined R&D and outreach activities, Meet. Abstr. (2021) 1556, https://doi.org/10.1149/MA2021-01571556mtgabs. MA2021-01.
[7] Y. Feng, X. Tian, Y. Chen, Z. Wang, J. Xia, J. Qian, Y. Zhuang, J. Chu, Real-time and on-line monitoring of ethanol fermentation process by viable cell sensor and electronic nose, Bioresour. Bioprocess. 8 (2021) 37, https://doi.org/10.1186/s40643-021-00391-5.
[8] P. Salgado, L. Di Giorgio, Y. Musso, A. Mauri, Recent developments in smart food packaging focused on biobased and biodegradable polymers, Front. Sust. Food Syst. 5 (2021), 630393, https://doi.org/10.3389/fsufs.2021.630393.
[9] S. Zhan, D. Li, S. Liang, X. Chen, X. Li, A novel flexible room temperature ethanol gas sensor based on SnO2 doped poly-diallyldimethylammonium chloride, Sensors 13 (2013) 4378–4389, https://doi.org/10.3390/s130404378.
[10] S. Hu, G. Yan, C. Wu, S. He, An ethanol vapor sensor based on a microfiber with a quantum-dot gel coating, Sensors 19 (2019) 300, https://doi.org/10.3390/s19020300.
[11] Y. Luo, A. ly, D. Lahem, C. Zhang, M. Debliquy, A novel low-concentration isopropanol gas sensor based on Fe-doped ZnO nanoneedles and its gas sensing mechanism, J. Mater. Sci. 56 (2021) 1–16, https://doi.org/10.1007/s10853-020-05453-1.
[12] R. Capuano, M. Santonico, G. Pennazza, S. Ghezzi, E. Martinelli, C. Roscioni, G. Lucantoni, G. Galluccio, R. Paolesse, C. Di Natale, A. D'Amico, The lung cancer breath signature: a comparative analysis of exhaled breath and air sampled from inside the lungs, Sci. Rep. 5 (2015) 16491, https://doi.org/10.1038/srep16491.
[13] X. Min, W. Qin, X. Zhang, J. Fan, X. Zhu, Y. Zhu, X. Wang, J. Qiu, Y. Wang, X. Hu, M. Wei, W. Zhang, An ultra-high sensitive ethanol sensor through amending surface-functionalized groups by novel acidic synthesis methods, Sens. Actuators B Chem. 347 (2021), 130654, https://doi.org/10.1016/j.snb.2021.130654.
[14] Y.-Z. Li, Q.-J. Feng, B. Shi, C. Gao, D.-Y. Wang, H.-W. Liang, Room temperature non-balanced electric bridge ethanol gas sensor based on a single ZnO microwire, Chin. Phys. B. 29 (2020), 018102, https://doi.org/10.1088/1674-1056/ab593f.
[15] T.T. Suzuki, T. Ohgaki, Y. Adachi, I. Sakaguchi, M. Nakamura, H. Ohashi, A. Aimi, K. Fujimoto, Ethanol gas sensing by a Zn-Terminated ZnO(0001) bulk single-crystalline substrate, ACS Omega 5 (2020) 21104–21112, https://doi.org/10.1021/acsomega.0c02750.
[16] H. Ahmadvand, A. Iraji zad, R. Mohammadpour, S.H. Hosseini-Shokouh, E. Asadian, Room temperature and high response ethanol sensor based on two dimensional hybrid nanostructures of WS2/GONRs, Sci. Rep. 10 (2020) 14799, https://doi.org/10.1038/s41598-020-71695-3.
[17] N. Peng, Q. Zhang, C.L. Chow, O.K. Tan, N. Marzari, Sensing mechanisms for carbon nanotube based NH3 gas detection, Nano Lett. 9 (2009) 1626–1630, https://doi.org/10.1021/nl803930w.
[18] G. Ramanathan, K.R. Murali, Optical performance of Tin doped Indium Oxide (ITO) thin films prepared by sol gel dip coating techniques using acrylamide route, Opt. Quantum Electron. 54 (2022) 652, https://doi.org/10.1007/s11082-022-03973-5.
[19] Y. Sun, M. Sun, D. Xie, 5 - graphene electronic devices, in: H. Zhu, Z. Xu, D. Xie, Y. Fang (Eds.), Graphene, Academic Press, 2018, pp. 103–155, https://doi.org/10.1016/j.mtadv.2020.100060.
[20] B.Deka Boruah, Zinc oxide ultraviolet photodetectors: rapid progress from conventional to self-powered photodetectors, Nanoscale Adv. 1 (2019) 2059–2085, https://doi.org/10.1039/C9NA00130A.
[21] L. Zhu, W. Zeng, Room-temperature gas sensing of ZnO-based gas sensor: a review, Sens. Actuator A Phys. 267 (2017) 242–261, https://doi.org/10.1016/j.sna.2017.10.021.
[22] Z. Jing, J. Zhan, Fabrication and gas-sensing properties of porous ZnO nanoplates, Adv. Mater. 20 (2008) 4547–4551, https://doi.org/10.1002/adma.200800243.
[23] Z.Q. Zheng, J.D. Yao, B. Wang, G.W. Yang, Light-controlling, flexible and transparent ethanol gas sensor based on ZnO nanoparticles for wearable devices, Sci. Rep. 5 (2015) 11070, https://doi.org/10.1038/srep11070.
[24] M. Aleksanyan, A. Sayunts, G. Shahkhatuni, Z. Simonyan, G. Shahnazaryan, V. Aroutiounian, Gas sensor based on ZnO nanostructured film for the detection of ethanol vapor, Chemosensors 10 (2022) 245, https://doi.org/10.3390/chemosensors10070245.
[25] M. Thanihaichelvan, Highly sensitive and selective ethanol sensor based on ZnO Nanorod on SnO2 thin film fabricated by spray pyrolysis, Front. Mater. 6 (2019), https://doi.org/10.3389/fmats.2019.00122.
[26] S. Zhang, Z. Liu, L. Zhang, J. Chen, Q. Zhou, H. Zhang, L. Nie, Z. Dong, Z.a. Zhang, Z. Wang, G. Pan, Construction of a low-temperature, highly sensitive H2S sensor based on surfaces and interfaces reaction triggered by Au-doped hierarchical structured composites, Chem. Phys. Lett. 763 (2021), 138188, https://doi.org/10.1016/j.cplett.2020.138188.
[27] Y. Kang, L. Zhang, W. Wang, F. Yu, Ethanol sensing properties and first principles study of au supported on mesoporous ZnO Derived from Metal Organic Framework ZIF-8, Sensors 21 (2021) 4352, https://doi.org/10.3390/s21134352.
[28] Y.-S. Tsai, S.C. Tsai, C.C. Kuo, W.L. Chan, W.H. Lin, Y.S. Wu, Y.S. Lin, M.H. Li, M.-Y. Kuo, H. Chen, Organic/inorganic hybrid nanostructures of polycrystalline perylene diimide decorated ZnO nanorods highly enhanced dual sensing performance of UV light/CO gas sensors, Results Phys. 24 (2021), 104173, https://doi.org/10.1016/j.rinp.2021.104173.
[29] Y. Kang, F. Yu, L. Zhang, W. Wang, L. Chen, Y. Li, Review of ZnO-based nanomaterials in gas sensors, Solid State Ion 360 (2021), 115544, https://doi.org/10.1016/j.ssi.2020.115544.
[30] J. Cheng, D. Hu, A. Yao, Y. Gao, H. Asadi, A computational study on the Pd-decorated ZnO nanocluster for H2 gas sensing: a comparison with experimental results, Physica E Low Dimens. Syst. Nanostruct. 124 (2020), 114237, https://doi.org/10.1016/j.physe.2020.114237.
[31] V. Aroutiounian, Decrease in Operation Temperature of Zinc Oxide Nanomarkers, Biomed. J. Sci. Technol. Res. 30 (2020), https://doi.org/10.26717/BJSTR.2020.30.004919.
[32] S.H. Park, S.M. Lee, E.H. Ko, T.H. Kim, Y.C. Nah, S.J. Lee, J.H. Lee, H.K. Kim, Roll-to-Roll sputtered ITO/Cu/ITO multilayer electrode for flexible, transparent thin film heaters and electrochromic applications, Sci. Rep. 6 (2016) 33868, https://doi.org/10.1038/srep33868.
[33] Y. Zhou, R. Azumi, Carbon nanotube based transparent conductive films: progress, challenges, and perspectives, Sci. Technol. Adv. Mater. 17 (2016) 493–516, https://doi.org/10.1080/14686996.2016.1214526.
[34] J. Linnet, A.R. Walther, C. Wolff, O. Albrektsen, N.A. Mortensen, J. Kjelstrup-Hansen, Transparent and conductive electrodes by large-scale nano-structuring of noble metal thin-films, Opt. Mater. Express 8 (2018) 1733–1746, https://doi.org/10.1364/OME.8.001733.
[35] A. Alshammari, M.R. Alenezi, K.T. Lai, S.R.P. Silva, Inkjet printing of polymer functionalized CNT gas sensor with enhanced sensing properties, Mater. Lett. 189 (2017) 299–302, https://doi.org/10.1016/j.matlet.2016.11.033.
[36] S.S. Shaker, R.A. Ismail, D.S. Ahmed, High-responsivity heterojunction photodetector based on Bi2O3-Decorated MWCNTs nanostructure grown on silicon

via laser ablation in liquid, J. Inorg. Organomet. Polym. Mater. 32 (2022) 1381–1388, https://doi.org/10.1007/s10904-021-02199-4.
[37] Z. Wu, Z. Chen, X. Du, J.M. Logan, J. Sippel, M. Nikolou, K. Kamaras, J. R. Reynolds, D.B. Tanner, A.F. Hebard, A.G. Rinzler, Transparent, conductive carbon nanotube films, Science 305 (2004) 1273–1276, https://doi.org/10.1126/science.1101243.
[38] A.S. Pillai, A. Chandran, S.K. Peethambharan, MWCNT Ink with PEDOT:PSS as a multifunctional additive for energy efficient flexible heating applications, Appl. Mater. Today 23 (2021), 100987, https://doi.org/10.1016/j.apmt.2021.100987.
[39] Q. Huang, Y. Zhu, Printing conductive nanomaterials for flexible and stretchable electronics: a review of materials, processes, and applications, Adv. Mater. Technol 4 (2019), 1800546, https://doi.org/10.1002/admt.201800546.
[40] G. Kozma, R. Puskás, I.Z. Papp, P. Bélteky, Z. Kónya, Á. Kukovecz, Experimental validation of the Burgio–Rojac model of planetary ball milling by the length control of multiwall carbon nanotubes, Carbon 105 (2016) 615–621, https://doi.org/10.1016/j.carbon.2016.05.005.
[41] Y. Battie, O. Ducloux, P. Thobois, N. Dorval, J.S. Lauret, B. Attal-Trétout, A. Loiseau, Gas sensors based on thick films of semi-conducting single walled carbon nanotubes, Carbon 49 (2011) 3544–3552, https://doi.org/10.1016/j.carbon.2011.04.054.
[42] I.Z. Papp, G. Kozma, R. Puskás, T. Simon, Z. Kónya, Á. Kukovecz, Effect of planetary ball milling process parameters on the nitrogen adsorption properties of multiwall carbon nanotubes, Adsorption 19 (2013) 687–694, https://doi.org/10.1007/s10450-013-9493-8.
[43] N.M. Shaalan, F. Ahmed, M. Rashad, O. Saber, S. Kumar, A. Aljaafari, A. Ashoaibi, A.Z. Mahmoud, M. Ezzeldien, Low-temperature ethanol sensor via defective multiwalled carbon nanotubes, Materials 15 (2022), https://doi.org/10.3390/ma15134439.
[44] M. Farbod, M.H. Joula, M. Vaezi, Promoting effect of adding carbon nanotubes on sensing characteristics of ZnO hollow sphere-based gas sensors to detect volatile organic compounds, Mater. Chem. Phys. 176 (2016) 12–23, https://doi.org/10.1016/j.matchemphys.2016.03.004.
[45] R. Hegde, K. Ramji, S. Peravali, Y. Shiralgi, G. Hegde, L. Bathini, Characterization of MWCNT-PEDOT: PSS Nanocomposite flexible thin film for piezoresistive strain sensing application, Adv. Polym. Technol. 2019 (2019), 9320976, https://doi.org/10.1155/2019/9320976.
[46] S.F. Boscarino, G. Nicotra, S. Libertino, M. Scuderi, S.S. Galati, Investigation of ZnO-decorated CNTs for UV light detection applications, J. Nanomater. 9 (2019) 1099, https://doi.org/10.3390/nano9081099.
[47] R. Balint, N.J. Cassidy, S.H. Cartmell, Conductive polymers: towards a smart biomaterial for tissue engineering, Acta Biomater. 10 (2014) 2341–2353, https://doi.org/10.1016/j.actbio.2014.02.015.
[48] H. Shirakawa, E.J. Louis, A.G. MacDiarmid, C.K. Chiang, A.J. Heeger, Synthesis of electrically conducting organic polymers: halogen derivatives of polyacetylene, (CH), Chem. Commun. (1977) 578–580, https://doi.org/10.1039/C39770000578.
[49] Y. Wang, W. Jia, T. Strout, Y. Ding, Y. Lei, Preparation, characterization and sensitive gas sensing of conductive core-sheath TiO2-PEDOT nanocables, Sensors 9 (2009) 6752–6763, https://doi.org/10.3390/s90906752.
[50] L. Kinner, M. Bauch, R.A. Wibowo, G. Ligorio, E.J.W. List-Kratochvil, T. Dimopoulos, Polymer interlayers on flexible PET substrates enabling ultra-high performance, ITO-free dielectric/metal/dielectric transparent electrode, Mater. Des. 168 (2019), 107663, https://doi.org/10.1016/j.matdes.2019.107663.
[51] I.Z. Papp, A. Alegría, Z. Kónya, Á. Kukovecz, Investigation into the effect of ZnO nanorod coating on the thermal-mechanical and dielectric properties of ITO coated PET, Mater. Res. Bull. 149 (2022), 111701, https://doi.org/10.1016/j.materresbull.2021.111701.
[52] O. Kanoun, C. Müller, A. Benchirouf, A. Sanli, T.N. Dinh, A. Al-Hamry, L. Bu, C. Gerlach, A. Bouhamed, Flexible carbon nanotube films for high performance strain, Sensors 14 (2014) 10042–10071, https://doi.org/10.3390/s140610042.
[53] H. Kim, Y. Jang, G.W. Lee, S.Y. Yang, J. Jung, J. Oh, Tunable chemical grafting of three-dimensional poly (3, 4-ethylenedioxythiophene)/Poly (4-styrenesulfonate)-multiwalled carbon nanotubes composite with faster charge-carrier transport for enhanced gas sensing performance, 20 (2020) 2470. 10.3390/s20092470.
[54] N. Halonen, A. Sápi, L. Nagy, R. Puskás, A.-.R. Leino, J. Mäklin, J. Kukkola, G. Tóth, M.-.C. Wu, H.-.C. Liao, W.-.F. Su, A. Shchukarev, J.-.P. Mikkola, Á. Kukovecz, Z. Kónya, K. Kordás, Low-temperature growth of multi-walled carbon nanotubes by thermal CVD, Phys. Status Solidi B 248 (2011) 2500–2503, https://doi.org/10.1002/pssb.201100137.
[55] S. Baruah, J. Dutta, Hydrothermal growth of ZnO nanostructures, Sci. Technol. Adv. Mater. 10 (2009), 013001, https://doi.org/10.1088/1468-6996/10/1/013001.
[56] E. Kusiak-Nejman, J. Wojnarowicz, A.W. Morawski, U. Narkiewicz, K. Sobczak, S. Gierlotka, W. Lojkowski, Size-dependent effects of ZnO nanoparticles on the photocatalytic degradation of phenol in a water solution, Appl. Surf. Sci. 541 (2021), 148416, https://doi.org/10.1016/j.apsusc.2020.148416.
[57] B. Janett, A. Gutierrez, S. Dul, A. Pegoretti, J. Alvarez-Quintana, L. Fambri, Investigation of the effects of multi-wall and single-wall carbon nanotubes concentration on the properties of ABS nanocomposites, C, 7 (2021). 10.3390/c7020033.
[58] P. Bélteky, A. Rónavári, D. Zakupszky, E. Boka, N. Igaz, B. Szerencsés, I. Pfeiffer, C. Vágvölgyi, M. Kiricsi, Z. Kónya, Are smaller nanoparticles always better? Understanding the biological effect of size-dependent silver nanoparticle aggregation under biorelevant conditions, Int. J. Nanomed. 16 (2021) 3021–3040, https://doi.org/10.2147/IJN.S304138.
[59] M.-.S. Choi, T. Park, W.-.J. Kim, J. Hur, High-performance ultraviolet photodetector based on a zinc oxide Nanoparticle@Single-Walled carbon nanotube heterojunction hybrid film, J. Nanomater. 10 (2020) 395, https://doi.org/10.3390/nano10020395.
[60] C. Wang, L. Yin, L. Zhang, D. Xiang, R. Gao, Metal oxide gas sensors: sensitivity and influencing factors, Sensors 10 (2010) 2088–2106, https://doi.org/10.3390/s100302088.
[61] M. Zhao, H. Zhu, J. Zhang, M. Li, Z. Cai, Synthesis and gas sensor application of nanostructure Cr 2 O 3 hollow spheres, IOP Conf. Ser.: Mater. Sci. Eng. 207 (2017), 012030, https://doi.org/10.1088/1757-899X/207/1/012030.
[62] N. Ridha, F. Alosfur, M. Hj. Jumali, K. Taher, R. Madlool, N. Al-dahan, Ethanol sensor based on 1D and 2D ZnO nanostructures, AIP Conf. Proc. (2020) 2290, https://doi.org/10.1063/5.0027446.
[63] J. Liu, T. Wang, B. Wang, P. Sun, Q. Yang, X. Liang, H. Song, G. Lu, Highly sensitive and low detection limit of ethanol gas sensor based on hollow ZnO/SnO2 spheres composite material, Sens. Actuators B Chem. 245 (2017) 551–559, https://doi.org/10.1016/j.snb.2017.01.148.
[64] H.T. Hussein, M.H. Kareem, A.M. Abdul Hussein, Synthesis and characterization of carbon nanotube doped with zinc oxide nanoparticles CNTs-ZnO/PS as ethanol gas sensor, Optik (Stuttg) 248 (2021), 168107, https://doi.org/10.1016/j.ijleo.2021.168107.
[65] D. Sebők, L. Janovák, D. Kovács, A. Sápi, D.G. Dobó, Á. Kukovecz, Z. Kónya, I. Dékány, Room temperature ethanol sensor with sub-ppm detection limit: improving the optical response by using mesoporous silica foam, Sens. Actuators B. Chem. 243 (2017) 1205–1213, https://doi.org/10.1016/j.snb.2016.12.097.
[66] D. Sebők, I. Dékány, ZnO2 nanohybrid thin film sensor for the detection of ethanol vapour at room temperature using reflectometric interference spectroscopy, Sens. Actuators B. Chem. 206 (2015) 435–442, https://doi.org/10.1016/j.snb.2014.09.087.
[67] N. Yamazoe, New approaches for improving semiconductor gas sensors, Sens. Actuators B. Chem. 5 (1991) 7–19, https://doi.org/10.1016/0925-4005(91)80213-4.
[68] J. Guo, J. Zhang, M. Zhu, D. Ju, H. Xu, B. Cao, High-performance gas sensor based on ZnO nanowires functionalized by Au nanoparticles, Sens. Actuators B. Chem. 199 (2014) 339–345, https://doi.org/10.1016/j.snb.2014.04.010.
[69] C. Chang, M. Hon, I.-.C. Leu, Influence of size and density of Au nanoparticles on ZnO nanorod arrays for sensing reducing gases, J. Electrochem. Soc. 160 (2013) B170–B176, https://doi.org/10.1149/2.076309jes.
[70] N. Donato, M. Latino, G. Neri, Novel carbon nanotubes-based hybrid composites for sensing applications. Carbon Nanotubes, Intech Open, 2011, https://doi.org/10.5772/18855.
[71] S. Zhang, P. Kumar, A. Nouas, F. Laurie, H. Tang, F. Cicoira, Solvent-induced changes in PEDOT: PSS films for organic electrochemical transistors, APL Mater. 3 (2014), 014911, https://doi.org/10.1063/1.4905154.
[72] B.K. Sharma, N. Khare, S. Ahmad, A ZnO/PEDOT:PSS based inorganic/organic hetrojunction, Solid State Commun. 149 (2009) 771–774, https://doi.org/10.1016/j.ssc.2009.02.035.
[73] R.A. Talib, M.J. Abdullah, H.S. Al-Salman, S.M. Mohammad, N.K. Allam, ZnO nanorods/polyaniline heterojunctions for low-power flexible light sensors, Mater. Chem. Phys. 181 (2016) 7–11, https://doi.org/10.1016/j.matchemphys.2016.06.061.
[74] J. Ghushe, S. Kondawar, Fabrication of inorganic/organic hybrid heterojunctions of polyaniline composite/blend for the study of diode characteristics, J. Phys. Sci. 28 (2016) 99–109, https://doi.org/10.21315/jps2017.28.8.
[75] M. Sinha, S. Neogi, R. Mahapatra, S. Krishnamurthy, R. Ghosh, Material dependent and temperature driven adsorption switching (p- to n- type) using CNT/ZnO composite-based chemiresistive methanol gas sensor, Sens. Actuators B Chem. 336 (2021), 129729, https://doi.org/10.1016/j.snb.2021.129729.
[76] M.H. Kareem, H.T. Hussein, A.M. Abdul Hussein, Study of the effect of CNTs, and (CNTs-ZnO) on the porous silicon as sensor for acetone gas detection, Optik (Stuttg) 259 (2022), 168825, https://doi.org/10.1016/j.ijleo.2022.168825.
[77] R.D. Ladhe, K.V. Gurav, S.M. Pawar, J.H. Kim, B.R. Sankapal, p-PEDOT:PSS as a heterojunction partner with n-ZnO for detection of LPG at room temperature, J. Alloy. Compd. 515 (2012) 80–85, https://doi.org/10.1016/j.jallcom.2011.11.076.
[78] D.S. Dhawale, R.R. Salunkhe, U.M. Patil, K.V. Gurav, A.M. More, C.D. Lokhande, Room temperature liquefied petroleum gas (LPG) sensor based on p-polyaniline/n-TiO2 heterojunction, Sens. Actuators B Chem. 134 (2008) 988–992, https://doi.org/10.1016/j.snb.2008.07.003.
[79] G. Lu, L. Ocola, J. Chen, Reduced graphene oxide for room-temperature gas sensors, Nanotechnology 20 (2009), 445502, https://doi.org/10.1088/0957-4484/20/44/445502.
[80] M. Shooshtari, S. Pahlavan, S. Rahbarpour, H. Ghafoorifard, Investigating organic vapor sensing properties of composite carbon nanotube-zinc oxide nanowire, Chemosensors 10 (2022) 205, https://doi.org/10.3390/chemosensors10060205.
[81] M. Rana, S. Dauda, M.A. Mohd Razib, S. Jarin, A.N.M. Tomal, A review on recent advances of CNTs as gas sensors, Sensor Rev. 37 (2017) 127–136, https://doi.org/10.1108/SR-10-2016-0230.
[82] N.L.W. Septiani, B. Yuliarto, H.K.D. Nugraha, Multiwalled carbon nanotubes–zinc oxide nanocomposites as low temperature toluene gas sensor, Appl. Phys. A 123 (2017) 166, https://doi.org/10.1007/s00339-017-0803-y.